fluids

MDPI

Article

Laser-Plasma Accelerated Protons: Energy Increase in Gas-Mixtures Using High Mass Number Atomic Species

Tadzio Levato [1,*], Leonardo V. Goncalves [1] and Vincenzo Giannini [2,3]

[1] Institute of Physics of the ASCR, ELI Beamlines Project, Na Slovance 2, 18221 Prague, Czech Republic
[2] Instituto de Estructura de la Materia (IEM), Consejo Superior de Investigaciones Científicas (CSIC), Serrano 121, 28006 Madrid, Spain
[3] The Blackett Laboratory, Imperial College London, London SW7 2AZ, UK
* Correspondence: tadzio.levato@gmail.com; Tel.: +420-601-555-061

Received: 20 June 2019; Accepted: 31 July 2019; Published: 8 August 2019

Abstract: The idea of using a gas-mixture comprising atoms with a high mass number in order to increase proton energies in laser induced plasma acceleration at critical density is investigated by means of 2D PIC (Particle-In-Cell) simulations. Comparing and discussing the case of a pure hydrogen plasma and that of a plasma containing higher mass number species with a small percentage of hydrogen, we demonstrate that the mixture enhances the energies of the accelerated protons. We also show that using a gas-mixture introduces the possibility of using the densities ratio in order to change the relative acceleration of the species.

Keywords: proton acceleration; high density gas-jet; gas-mixture; laser wake-field acceleration (LWFA)

1. Introduction

After the advent of the Chirped-Pulse-Amplification (CPA) method [1], the growing interest in high power femtosecond laser systems has led to experiments aimed at using laser-matter interaction for particle acceleration. The use of the so-called Laser Wake-Field Acceleration (LWFA) technique [2] has led to the production of about 8 GeV electrons over very short distances of roughly 10 cm [3] in under-critical plasma using gas-filled capillaries. The use of the entitled TNSA (Target Normal Sheath Acceleration) has generated up to 100 MeV proton bunches in over-critical plasmas using solid targets [4].

The intermediate range of near-critical density (NCD) plasmas has also been experimentally used to accelerate ions at the plasma output interface (refer to Figure 1 and the caption for the description of "plasma output" and "input"). Typically, such densities of 10^{19}–10^{21} e^{-}/cm^{3} were reached by pre-illuminating a solid target so as to generate an expanding pre-plasma region [5], or by operating precise high density gas-jets [6].

Over the last few decades, laser proton acceleration was mainly performed in over-critical plasmas using solid targets that are understandably locally destroyed during the final phase of the process [7]. Using solid targets to work above the critical density results, therefore, in the introduction of a limiting factor in the repetition rate of the entire process, which is due to the need to refresh the target surface after every single laser shot. The possibility arising from the use of a gas-jet, capable of operating at a high repetition rate, or even in a continuous-flux mode, provides a significant contribution to overcome the limiting factor affecting the repetition rate of the process. Moreover, the use of high density gas-jet to accelerate protons at near under-critical density plasmas is also interesting from the view point of physics, since it offers an alternative method to the use of very high electric fields acting

for a very short period of time, which nowadays represents the usual approach of interaction with solid targets: the possibility of using moderate but longer lasting electric fields.

The discussion following [6] points out that two main mechanisms [8,9] can be identified as playing a role in the proton acceleration following the interaction of an under-critical target with high power pulse:

i. one is the acceleration due to the electrostatic field related to space charge effects (SCE),
ii. the other one is the acceleration due to the induced electric field related to "magnetic vortex acceleration" (MVA).

In particular, it was shown [9] that acceleration due to the electrostatic field was 2/3 of the total accelerating field in [6]. Additional works have shown experimental results in near-critical over-dense plasmas [10] using very thin plasma. The near critical condition also needed investigation of the propagation properties of the high intensity laser in such a thin plasma [11]. These studies have shown an increased efficiency in the proton acceleration mechanism for slightly under-critical plasma (0.9 n_c). Similar works [12] confirmed the importance of the time varying fields at the plasma output and also in the case of ions using gas-cluster target [13,14]. Such time varying fields have been shown to be enhanced by increasing the hot electron transport at high energies, resulting in a rapid generation of magnetic fields at the plasma output [15]. The use of particularly thin plasma slabs, obtained by collisionless plasma shock, resulted in the acceleration of mono-energetic protons [16] and in the identification of the density range needed to accelerate collimated ions [17], also opening the possibility to increase the particle energy using a staged acceleration concept [18] and improving the quality of the accelerated bunch tailoring the plasma profile [19]. Other works have experimentally investigated on solid targets the use of mixed species plasma [20,21], the role of nanostructure on the front-surface [22], and the role of coating on the rear-surface [23]. All the above-mentioned studies are important to improve the efficiency of a laser-plasma proton accelerator.

The interest in a laser-based proton accelerator covers different fields, from the most demanding hadron-therapy [24,25] extensively studied in literature and requiring high-energy protons (250 MeV), to the proton-induced-x-ray-emission (PIXE) technique [26]. In this case, a proton bunch irradiates a sample to induce X-ray fluorescence [27] in a localized region of the sample, the X-rays are then imaged using dedicated pin-hole cameras techniques [28–30] which are able to image X-ray, including in extreme conditions such as those met in laser-plasmas interactions. Such techniques have allowed for the study of fast electron dynamics [31], specifically thanks to the adopted method of counting the single X-ray photons [32,33]. The concept of all-optical radiation sources [34] is widely used in laser-based under-dense plasma electron accelerators, since this is a great advantage for medium and small scale research laboratories [35,36]. This technique offers the possibility to irradiate samples with a wide range of applications, from industry to biomedics.

In the present paper, we focus on the proton acceleration mechanism in under-critical plasma regimes. Working with under-critical plasma is advantageous for a few practical reasons: the flexibility of the repetition rate, as anticipated before, the simplicity in monitoring the interaction during the propagation [37], and, as we will consider below in the text, for the flexibility to mix different atomic species, having the possibility to arbitrary tune their relative densities. Experimental tests on proton acceleration have also demonstrated the possibility to use kHz laser, which offers an important advantage in term of compactness and versatility of the source [38,39] using liquid targets. Different projects and research centers base their activity on the concept of plasma-acceleration, and we should mention, in particular, the case of ELI [40] and some of the acceleration infrastructures within it [41,42].

2. The Aim of This Study and Outline

In this paper, we examine the possibility of using a gas-mixture for near-under-critical proton acceleration in laser-plasma interaction, introducing heavier atoms than hydrogen in the background plasma. A similar idea, using solid-targets, was proposed in [21]. Here, we reconsider the two

acceleration mechanism identified in [6,8,9] (points (i) and (ii) above) by investigating the role in proton acceleration played by a plasma mixture containing high mass number ions. In fact, since the heavier ions move slower than protons, they allow for the space charge effect at the plasma output to survive for longer times. This allows a longer acceleration time of the protons by the background plasma. The use of heavier atomic species in a gas-target introduces a new feature regarding the control of the acceleration of the lighter ions: i.e., the additional possibility of tuning the acceleration ratio by means of the density ratio of the species. This point will be discussed in the "modelling section" of this paper in which the results of 2D-PIC (Particle-In-Cell) simulations, meant as a simplified "virtual experiment", are analyzed. The analysis will focus on the discussion of the two mechanisms identified above in a simplified setting, which privileges a fluid description (see Sections 5 and 6).

In particular, the first part of the analysis will describe the electrostatic acceleration ratio of the two species in a multi-fluid description: once the ultrarelativistic electrons escape from the plasma, the latter remains positively charged, hence pushing the protons.

However, differently from the solid-target case [21] in which only a capacitor-like acceleration mechanism takes place, the gas-target case (under-critical case), as already described in [6–9], means the two mechanisms (i) and (ii) coexist. This is because the ultrarelativistic electron population rapidly generates a magnetic vortex structure at the plasma edge (which we will call "output"—see Section 3), which induces an electric field that further accelerates the protons.

The second part of the modelling focuses on the acceleration ratio of the two species due to the induced fields.

3. Numerical Models and Simulation Setup

The laser-plasma interaction was simulated by means of the 2D PIC code EPOCH [43] using a basic scenario, in which two different atomic species were involved. The intent was to keep the study as close to a realistic experimental case as possible.

The idea of using different atomic species in the background plasma is considered in ideal conditions. In the present cases, a flat density plasma with a step-like transition from vacuum to plasma was used in combination with a decreasing density at the plasma output. The laser entered at the left side of the simulation box, which we will name hereafter "plasma input". The right edge will hereafter be named "plasma output". The high intensity laser pulse pushes the electrons by means of the ponderomotive force during the propagation (see Figure 1).

The 2D PIC numerical box was 220 μm long and 40 μm wide. From left to right, the first 120 μm (plus the initial −20 μm) consisted of a flat density plasma, whereas the last 80 μm were used to decrease the density to zero by using a half-Gaussian profile. This basic density profile was used in order to put emphasis on the plasma output where the proton acceleration takes place, and this was obtained considering a plasma output profile more similar to the one associated to a real case rather than a simple ideal step-like transition. On the other hand, as the input plasma profile mainly affects the focusability of the laser pulse (of which a study is beyond the scope of this article), an ideal step-like transition was therefore considered at the input plasma profile. The convolutional perfectly matched layer boundary conditions were used in all the 2D-PIC simulations (see reference [43] and references therein). All the simulations presented here were carried out with a spatial resolution of $\lambda/20$ in both directions, with 12 particles per cell, using a λ = 800 nm linearly polarized laser pulse with a peak intensity of 10^{20} W/cm^2. All the simulations performed were stopped after 1ps from the beginning of the interaction (if not explicitly stated differently), giving only a partial indication of the final energy of the accelerated particles.

The idea was to study a common experimental case of a focal spot around 3 μm Full-Width at Half-Maximum (FWHM) using 1 J-class, 30 femtosecond laser (the case of a 10–30 TW femtosecond laser system) pulse as shown in the conceptual setup of Figure 1.

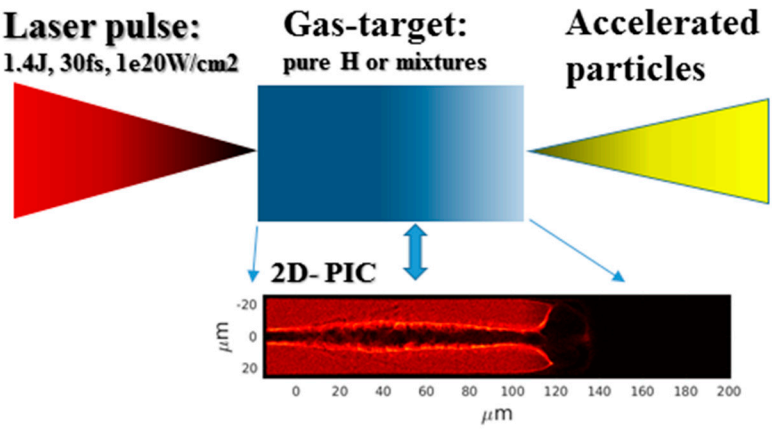

Figure 1. Conceptual setup of the experiment simulated into the 2D-PIC (Particle-In-Cell). The laser, consisting of 1.4 J energy, 30 fs pulse duration and of which focused on a focal spot of 3 μm-FWHM (Full-Width at Half-Maximum) to reach a peak intensity of 10^{20} W/cm^2, enters at the left side, which we will name hereafter "plasma input". The right edge will hereafter be named "plasma output".

In order to verify the effect of the background plasma density, as well as to select the best case for the subsequent comparison with the plasma-mixture case, our starting point was to consider pure hydrogen plasmas. We note that we ran a large number of simulations using different gas-mixtures which confirmed the validity of the idea of using higher mass number ions in order to enhance proton acceleration. Among these simulations, however, only the most relevant cases that are useful to prove these results are shown in the following. Additional investigation bearing in mind the output scale length plasma density and the optimal balance between the hydrogen fractions (%) in the gas mixture may contribute to further optimizing the process.

Such an optimal percentage will of course depend on the specific case of ion acceleration to be considered (for example, the He and C ions suitable for hadron-therapy).

4. Results of the 2D-PIC

4.1. The Case of Pure Hydrogen

Figure 2 shows the comparison of two snapshots of the laser plasma interaction at different plasma densities after 1000 fs from the pulse entry (−20 μm) in the simulation box (so that the laser pulse has already left the simulated model's area). The electrons (frames a) and protons (frames b) density distributions are shown for both pure hydrogen plasmas, respectively, at a flat density of 7×10^{19} e$^-$/cm^3 (left) and 2×10^{20} e$^-$/cm^3 (right). The frames (c) show the protons' (black) and the electrons' (green) energies versus the position along the axis of laser propagation. For both cases, the comparison shows energetic protons in the same region where density is decreasing and an increase of the proton energy as expected for the higher plasma density case, up to about 5 MeV maximum (at 1000 fs from the beginning of the interaction).

As it is clearly shown, the proton energy increases in the region in which the plasma density starts to decline (the region in between 100 and 150 micron). We should mention, however, that in the present paper, we are not interested in the study of the interdependence between the proton energy increase and the density decrease scale length. For this specific configuration, in the higher density case at 2×10^{20} e$^-$/cm^3 and 1000 fs after the beginning of the interaction (so that the laser pulse has already left the simulated model's area), the maximum proton energy approximately reaches a value of about 5 MeV, with the proton bunch longitudinally localized inside an interval of about 10 μm of the laser propagation axis. In particular, the proton energy increases from about 3 to 5 MeV, respectively, for the background plasma densities of 7×10^{19} and 2×10^{20} e$^-$/cm^3 (considered again at 1000 fs from the beginning of the interaction). An increase in the background plasma density (still for the case in which a pure hydrogen plasma is considered) would lead to a further noticeable energy increase. A too high

plasma density would instead prevent the laser propagation up to the "plasma output", inhibiting the entire proton acceleration process due to laser erosion.

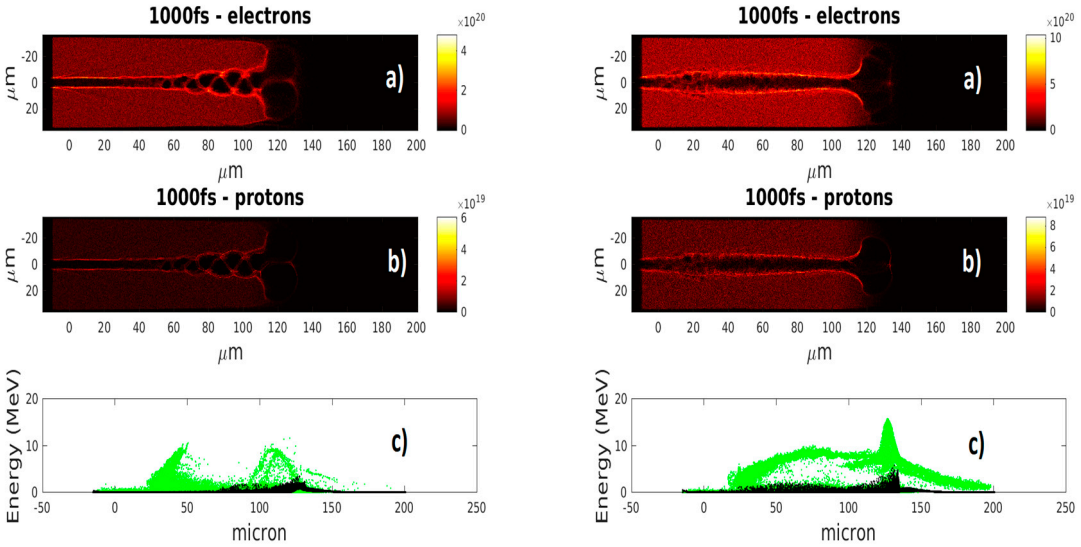

Figure 2. Snapshots of the 2D PICs after 1000 fs from the laser pulse entry in the simulation box of a pure hydrogen plasma at a flat density of 7×10^{19} e^-/cm^3 (**left**) and 2×10^{20} e^-/cm^3 (**right**). The electrons' (frames **a**) and protons' (frames **b**) density distributions are shown for both cases together with the protons' (black) and electrons' (green) energies versus the laser propagation direction (frames **c**).

Figure 3 shows the snapshot of the laser plasma interaction, taken after 1000 fs from the pulse entry in the simulation box in the case of a pure hydrogen plasma at a flat density of 7×10^{20} e^-/cm^3. As can be seen, in this case, the laser pulse is not capable of propagating over few tens of microns at such a plasma density, which inhibits the entire proton acceleration process.

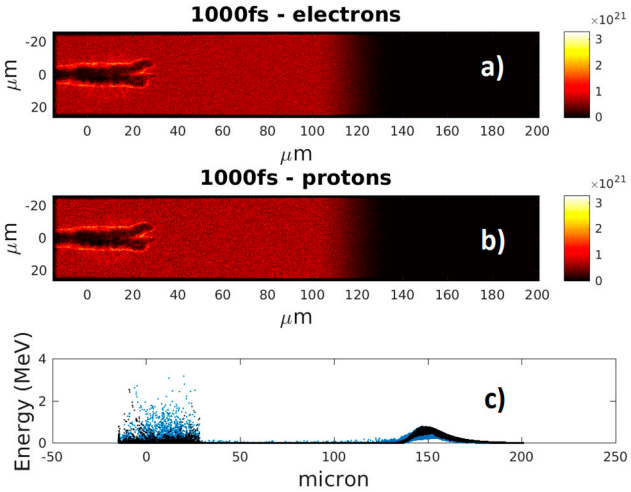

Figure 3. Snapshot of the 2D PIC after 1000 fs from the pulse entry in the simulation box of a pure hydrogen plasma at a flat density 7×10^{20} e^-/cm^3. The electrons' (frame **a**) and protons' (frame **b**) density distributions are shown for both cases, together with the protons' (black) and electrons' (blue) energies versus the laser propagation direction (frame **c**).

4.2. The Case of Hydrogen with a Heavier Species (Gas-Mixture)

For the comparison of the effect of different mass numbers atoms in the background plasmas, we used the same plasma profile both with respect to scale length and electron densities, which was considered in the previous case.

Xenon (Xe), with A = 131, stands out as a promising candidate in the selection process for a higher mass number noble gas (at room temperature and excluding the radioactive case of Radon) for the use of a gas-mixture-target. Nevertheless, also the cases of Kr, Ar, Ne, and N could be considered for proton acceleration. However, due to the role played by the atomic number in the acceleration process (which we will discuss in Section 5), the higher mass number case of Xe can be preferred to accelerate ions that are heavier than protons, such as He and C, which are both useful for hadron-therapy.

Figure 4 shows the snapshots of the laser-plasma interaction for a fully-ionized 95% Xe–5% H plasma mixture simulated by 2D PIC after 1000 fs from the pulse entry (−20 μm) in the simulation box (so that the laser pulse has already left area). For a simpler comparison with the case of Figure 2 (right), the total electron density is set to 2×10^{20} e^{-}/cm^{3} and the plasma profile considered is the same. The electrons' (frame a) and protons' (frame b) density distributions are shown with the protons' (black) and electrons' (green) energies versus the laser propagation direction (frame c). The proton energy reaches approximately the 10 MeV threshold at the plasma output, confirming that the simple use of higher mass number ions promotes the acceleration process with an energy increase of about a factor 2 (at 1 ps from the beginning of the interaction) when compared with the pure hydrogen case, still at the same electronic density and plasma profile.

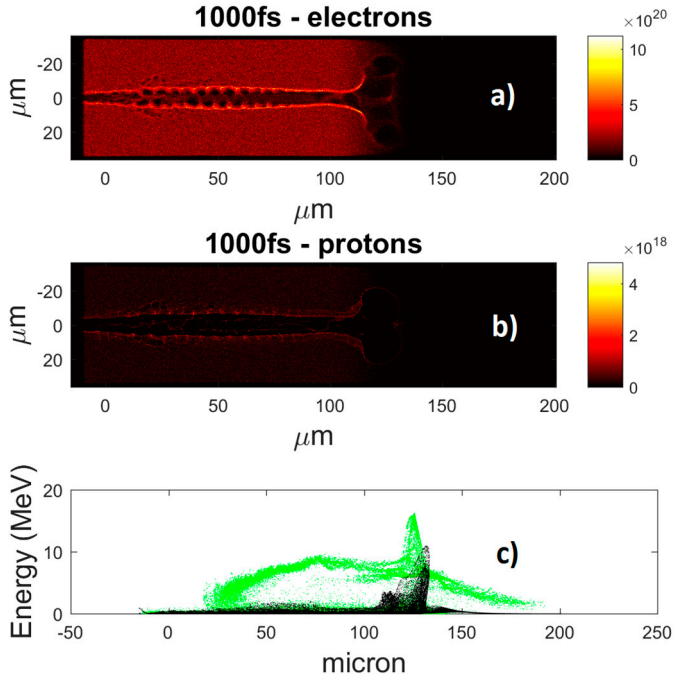

Figure 4. Snapshots of the 2D PICs after 1000 fs from the laser pulse entry in the simulation box of a fully-ionized 95% Xe–5% H plasma mixture at a flat density of 2×10^{20} e^{-}/cm^{3} for a comparison with the case of Figure 2 (right). The electrons' (frame **a**) and protons' (frame **b**) density distributions are shown for both cases together with the protons' (black) and electrons' (green) energies along the laser propagation direction (frame **c**). An energy increase of about a factor 2 is evident with respect to the pure hydrogen plasma case (Figure 2 (right)).

As anticipated, even lower mass number atoms and gases more common than Xe can be used based on this idea of including different mass number atoms in order to promote the acceleration of the lighter atom population.

As an example, we also considered the case of Ar and N used to accelerate protons.

Figure 5 shows the snapshots of the laser-plasma interaction for two fully-ionized plasma mixtures, respectively 95%Ar–5%H (left frames) and 95%N–5%H (right frames). Again, we show the results after 1000 fs from the pulse entry (−20 μm) in the simulation box (so that the laser pulse has already left the area). The total electron density is set to be 2×10^{20} e^{-}/cm^{3} for a simpler comparison with the

case of Figure 2 (right), and the plasma profile considered is also the same. The electrons' (frames a) and protons' (frames b) density distributions are shown with the protons' (black) and electrons' (green) energies versus the laser propagation direction (frames c).

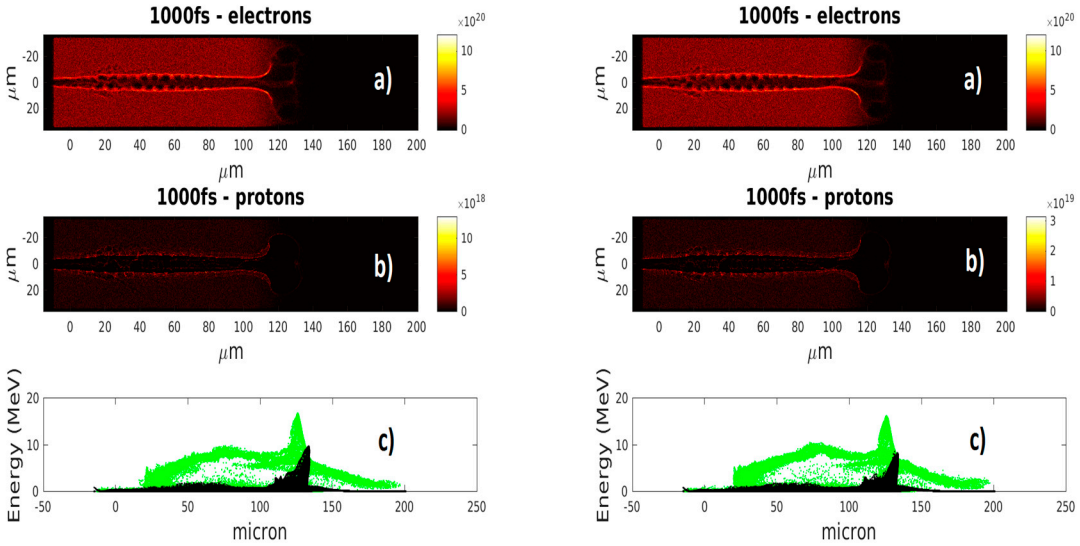

Figure 5. Shows the snapshots of the laser-plasma interactions for a fully-ionized 95%Ar–5%H (**left**) and 95%N–5%H (**right**) plasma mixture simulated by 2D PIC after 1000 fs from the pulse entry (−20 μm) in the simulation box (so that the laser pulse has already left the area). The total electron density is set to be 2×10^{20} e^{-}/cm^{3} for a simpler comparison with the case of Figure 2 (right). Also, the plasma profile considered is the same. The electrons' (frames **a**) and protons' (frames **b**) density distributions are shown with the protons' (black) and electrons' (green) energies versus the laser propagation direction (frames **c**).

The proton energy reaches approximately the value of 10 MeV at the plasma output, which leads to an energy increase of about a factor 2 when compared with the pure hydrogen case, still at the same electronic density and plasma profile (at 1000 fs from the beginning of the interaction).

We emphasize that in all the above mentioned 2D-PIC simulations, a proton density much smaller than the heavier atom density has been assumed.

5. Interpretation and Discussion: Acceleration Ratio of Two Different Species

In order to estimate the acceleration ratio of different plasma species, we consider the two main mechanisms at play in the proton acceleration as discussed in [6,8,9], by following an idealized scheme that privileges a fluid-like description.

The first mechanism (indicated as (i) above in the text) consists of the acceleration due to the electrostatic field derived from the space charge distribution. Since a bunch of electrons escapes from the plasma, the latter remains positively charged.

The second one (indicated as (ii) above in the text) consists of the acceleration due to the electric field induced by the magnetic vortex structure. The ultra-relativistic electrons escaping from the plasma generate a magnetic field that induces an electric field that further pushes the protons [44].

The proton acceleration takes place at the "plasma output" boundary due to these two distinct mechanisms as soon as the laser pulse and the ultra-relativistic electrons have already left the plasma. We consider such a phase of the process for the proton and heavier species in a fluid-like description.

In fact, since the laser pulse represents the only "driver" moving the system (the plasma under examination) out from the equilibrium that is capable of inducing kinetic effects on the electrons (as, for example, the wave-breaking mechanism), once the ultrashort laser pulse has left the plasma and the ultra-relativistic electrons travelling approximately at the speed of the light have done the same, the plasma remains without "external forces" applied.

As a consequence, the protons and the heavier species dynamics can be considered as a relaxation phase of the plasma, not anymore subjected to the strong external laser field. As a first approximation, we can then neglect kinetic effects.

For this reason, the physical mechanisms of acceleration we are discussing can be qualitatively illustrated by considering a neutral fluid element consisting of 3 fluid species: the electrons, the protons, and the heavier ions considered, with the respective numerical densities n_e, n_p, n_{Atom} and accelerations a_e, a_p, and a_{Atom}. The suffix "Atom" represents the atomic species in the gas-mixture with mass number A and atomic number Z. In the plasma, we assume it to be a fully ionized ion.

Additionally, since the protons and the heavier species, due to their higher inertia, move over a longer time scale with respect to the electrons taking part in the magnetic vortex structure, the induced electric field can be considered for their dynamics as an external field.

We will discuss in the next sub-sections an estimation of the instantaneous acceleration ratios of the ions and protons, which are due to the electrostatic effect owing to the space charge separation, and to the effect of the induced electric field owing to magnetic vortex.

It should be noted that these estimations are useful to identify and to qualitatively show the role played by the main parameters taking place in the acceleration mechanisms, but they are not quantitatively predictive due to the crude approximations done. In particular:

a. The specific geometry involved at the plasma output boundary where the mechanisms take place will not be considered (all the 2D-PIC Figures evidence the presence of a deep density channel on the laser propagation axis, which we are not going to consider).
b. The time evolution of the forces accelerating the ions (and of the quantities they depend on) should be obviously considered in order to quantify the final acceleration of each species.

Therefore, the scalings we will provide for the acceleration ratios are not expected to match the numerical result (indeed, as we will see, they provide an overestimate, although the trend of the scaling is confirmed by the simulations—see Sections 5 and 6).

Nevertheless, on the other hand, we can expect that the energy gain for the acceleration of the lighter species, which we have measured in our 2D PIC simulations, represents a lower bound of what should actually be obtained at the end of the process, since we only considered an early 1ps time interval (and further effects which later decelerate the lighter ion species more than the heavier ions are not expected in this configuration).

5.1. Acceleration Ratio from Space Charge Effect

Assuming the Coulombian repulsion (in the ideal conditions of fully ionized plasma in which all the electrons are suddenly removed), it follows from the action-reaction principle that the accelerating force applied to the two remaining species, namely protons and ions, within the same fluid element will instantaneously be the same. This leads to the estimate of the ratio between acceleration of the two species in the fluid elements as:

$$\frac{a_p}{a_{\mathrm{Atoms}}} = \frac{n_{\mathrm{Atoms}}}{n_p} A \tag{1}$$

where A is the mass number of the specific atomic species under consideration. As it is shown, Equation (1) clearly introduces two distinct ways of promoting the proton acceleration, a first one through the use of heavier atoms ($A >> 1$) and the other by changing the species' densities. From this simple description, an additional generalization to promote the acceleration of heavier ions can be made by simply considering a second atomic species instead of protons, following the formula:

$$\frac{a_{\mathrm{Atoms1}}}{a_{\mathrm{Atoms2}}} = \frac{n_{\mathrm{Atoms2}}}{n_{\mathrm{Atoms1}}} \frac{A_2}{A_1}. \tag{2}$$

Likewise, in Equation (2), the proton case is consistent with Equation (1), and also clearly shows two distinct ways to promote the acceleration of the atomic species referred to as "Atoms-2" with

respect to the atomic species "Atoms-1". This corresponds to either choosing a different mass number in order to modify their ratio or to change the densities of the species in order to promote the acceleration of one of them.

These equations are useful to see the scaling in this mechanism of the acceleration ratio with dimensionless parameters such as the instantaneous density ratio or the mass numbers. Nevertheless, these equations only offer a qualitative indication, as explained above. This means that such equations cannot be used as predictive of the final particles' energy. Moreover, since the simulations are stopped after 1ps from the beginning of the interaction when the acceleration mechanism is still acting, it is clear that the final particle energy in experiments will be higher. As an example, considering Equation (1) and the simulation described in Figure 4, Equation (1) clearly gives an estimate for the acceleration ratio of more than 2000 times the case of pure hydrogen; on the contrary, only a factor of 2 in energy gain is evident from the simulation due to the reasons mentioned above.

5.2. Acceleration Ratio from External Fields

This case is relevant to the so-called magnetic vortex acceleration [8]: i.e., an induced electric field that further pushes the protons and which is induced by the magnetic field generated by the fast electrons escaping from the plasma. We consider the ideal simplified case in which, since the fields are generated by the electrons, at a specific time, the ions feel such a field as an external one.

In this case, we can rewrite the equations for the acceleration of protons and heavier ions, thus yielding:

$$\frac{a_p}{a_{\text{Atoms}}} = \frac{A}{Z}. \tag{3}$$

Taking into account the arrangement of the terms of Equation (3), the relation is clear. Once the atomic species have been selected, Equation (3) gives a fixed value of accelerations due to the declined ratio of densities.

A similar generalization can be done for the case of two distinct heavier atomic species, as follows:

$$\frac{a_{\text{Atoms1}}}{a_{\text{Atoms2}}} = \frac{Z_1}{A_1}\frac{A_2}{Z_2}. \tag{4}$$

Equation (4), in close likeness to the proton case, shows that even if heavier species are used, the ratio of the magnetic vortex accelerations is fixed solely by the atomic and mass numbers.

6. An Ideal Case for Further Studies

As we previously mentioned, the estimations provided in Section 5, which we suggested in order to give an interpretation of the numerical results previously discussed (Section 4), are based on quite idealized modelling. Therefore, before reaching the stage of a practical implementation of the use of a gas mixture, so as to enhance the acceleration mechanism of protons, other aspects, such as the role of a realistic input density profile and the different ionization potentials of different species, need to be discussed. The appropriateness of the qualitative estimations provided in Section 5 are, however, supported by a further numerical example, which we discuss here, and which can lead to further investigations.

The simplified modelling of the previous sections points out the dependence of the scaling of a_p/a_{Atoms} as linked to dimensionless parameters, respectively:

n_{Atoms}/n_p, A (Equation (1)) and A/Z (Equation (3)).

In order to support the interpretation provided above, we consider ideal cases made solely for theoretical considerations. Let us consider a high mass number, for example $A = 131$ like for Xe, and let us artificially change the Z number so as to numerically verify the effect it has on the acceleration process. We present in this section the simulations performed for both an ideal artificial atomic species with $Z = 1$ and $A = 131$ (this can be the case of Xe^{+1}, that we refer to as "low charge specie"), and an ideal

artificial species of $Z = 131$ and $A = 131$ (this is a fully ionized hydrogen cluster, a case of practical interest [12–14], in the particular case of 131 atoms, which we refer to as "high charge specie").

As can be seen in Figure 6, the results of these simulations (run up to 1.1 ps) qualitatively confirm the trend indicated by Equations (1) and (3) as far as the dependence of the acceleration mechanisms on the parameters at play is concerned. Moreover, since the ratio of the accelerations is different for the two mechanisms in the presence of heavier atomic species, the main idea exemplified by this ideal case can be used to study the interplay between the magnetic vortex acceleration and the space charge effects. This will be the subject of a further study.

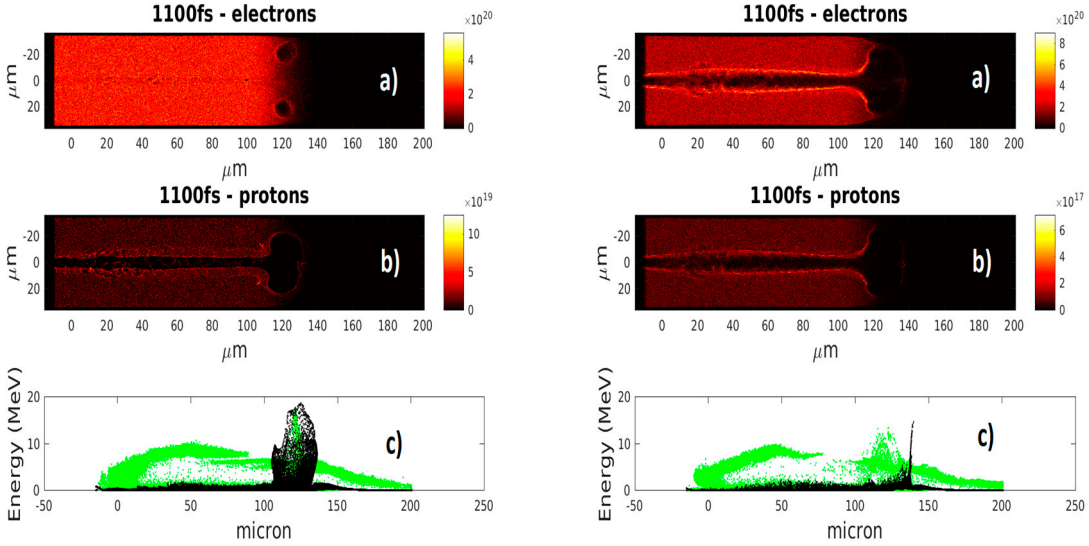

Figure 6. Shows the snapshots of the laser-plasma interactions, considering a fully-ionized artificial specie with $Z = 1$ and $A = 131$ that we call "low charge specie", in a mixture of 95% "low charge specie"–5%H (**left**) and a fully-ionized artificial specie with $Z = 131$ and $A = 131$ that we call "high charge specie", in a mixture of 95% "high charge specie"–5%H (**right**) plasma simulated by 2D PIC after 1100 fs from the pulse entry (−20 μm) in the simulation box (so that the laser pulse has already left the simulated model's area). The total electron density is set to be 2×10^{20} e^-/cm^3, and the plasma profile considered is the same. The electrons' (frames **a**) and protons' (frames **b**) density distributions are shown with the protons' (black) and electrons' (green) energies versus the laser propagation direction (frames **c**).

Figure 6 clearly shows an interesting method to study the interplay between magnetic vortex acceleration and space charge effects. However, such a study has to take into account the directionality of the accelerated particles if the aim is oriented towards practical applications. From this view point, even if in the maximum energy, the space charge repulsion can offer an advantage due to the possible use of the densities ratio in order to change the acceleration ratio, it is a non-directional mechanism. On the contrary, magnetic vortex acceleration induces directionality to the accelerated particle bunch. This represents only one of the examples that give an idea of a number of additional features to be considered in further studies and possible experimental investigations using gas-mixtures.

7. Conclusions

In this paper we investigated the idea of using gas-mixtures involving high mass number atomic species to promote proton acceleration in under-dense near critical laser-plasmas. The validity of such an idea has been verified using 2D-PIC simulations (performed with the code Epoch). Numerical results show an energy gain of about 2 with respect the pure hydrogen case in the time frame considered of 1 ps. A simple qualitative model was proposed for the dominant mechanism of acceleration, which in this regime is due to the space charge effects, and it was found that the advantage of such a mechanism

to promote the acceleration is due to the fact that the ratio of the densities of the heavier ions and protons can be tuned to boost the acceleration of the protons.

A basic generalization of such a model is presented, which leads to the possibility of using this concept so as to additionally accelerate heavier particles such as He and C.

Moreover, such a method has been qualitatively shown to give a different instantaneous acceleration ratio of the two ion species as far as the two different acceleration mechanisms are concerned, namely due to space charge effects and that of magnetic vortex acceleration. As a consequence, this offers a viable method for distinguishing these mechanisms in future experimental investigations.

Author Contributions: T.L. had the idea and performed the PIC simulations. L.V.G. contributed to the manuscript. V.G. contributed to the physical modelling.

Funding: This work has been supported by the Ministry of Education, Youth and Sports of the Czech Republic (project No. LQ1606) and by the projects "advanced research using high intensity laser produced photons and particles" (CZ.02.1.01/0.0/0.0/16_019/0000789) within the ADONIS-EAL (Electron Acceleration by Laser) and ADONIS-IAL (Ion Acceleration by Laser) research programs. VG acknowledge the Spanish Ministerio de Economia y Competitividad for financial support through the grant NANOTOPO (FIS2017-91413-EXP).

Acknowledgments: The first author thanks Daniele Del Sarto for his invaluable capability in stimulating discussions on the physical mechanisms. The first author thanks Daniele Margarone for his invaluable support in the "Particle acceleration by Laser" research program (RP3) at ELI-Beamline where the presented work was originally initiated.

Conflicts of Interest: The authors declare no conflict of interest.

References

1. Strickland, D.; Mourou, G. Compression of amplified chirped optical pulses. *Opt. Commun.* **1985**, *55*, 447–449. [CrossRef]
2. Tajima, T.; Dawson, J.M. Laser electron accelerator. *Phys. Rev. Lett.* **1979**, *43*, 267. [CrossRef]
3. Gonsalves, A.J.; Nakamura, K.; Daniels, J.; Benedetti, C.; Pieronek, C.; de Raadt, T.C.H.; Steinke, S.; Bin, J.H.; Bulanov, S.S.; van Tilborg, J.; et al. Petawatt Laser Guiding and Electron Beam Acceleration to 8 GeV in a Laser-Heated Capillary Discharge Waveguide. *Phys. Rev. Lett.* **2019**, *122*, 084801. [CrossRef] [PubMed]
4. Higginson, A.; Gray, R.J.; King, M.; Dance, R.J.; Williamson, S.D.R.; Butler, N.M.H.; Wilson, R.; Capdessus, R.; Armstrong, C.; Green, J.S.; et al. Near-100 MeV protons via a laser-driven transparency-enhanced hybrid acceleration scheme. *Nat. Commun.* **2018**, *9*, 724. [CrossRef] [PubMed]
5. Matsukado, K.; Esirkepov, T.; Kinoshita, K.; Daido, H.; Utsumi, T.; Li, Z.; Fukumi, A.; Hayashi, Y.; Orimo, S.; Nishiuchi, M.; et al. Energetic Protons from a Few-Micron Metallic Foil Evaporated by an Intense Laser Pulse. *Phys. Rev. Lett.* **2003**, *91*, 215001. [CrossRef] [PubMed]
6. Willingale, L.; Mangles, S.P.D.; Nilson, P.M.; Clarke, R.J.; Dangor, A.E.; Kaluza, M.C.; Karsch, S.; Lancaster, K.L.; Mori, W.B.; Najmudin, Z.; et al. Collimated Multi-MeV Ion Beams from High-Intensity Laser Interactions with Underdense Plasma. *Phys. Rev. Lett.* **2006**, *96*, 245002. [CrossRef] [PubMed]
7. Macchi, A.; Borghesi, M.; Passoni, M. Ion acceleration by superintense laser-plasma interaction. *Rev. Mod. Phys.* **2013**, *85*, 751. [CrossRef]
8. Bulanov, S.V.; Esirkepov, T.Z. Comment on "Collimated Multi-MeV Ion Beams from High-Intensity Laser Interactions with Underdense Plasma". *Phys. Rev. Lett.* **2007**, *98*, 049503. [CrossRef]
9. Willingale, L.; Mangles, S.P.D.; Nilson, P.M.; Clarke, R.J.; Dangor, A.E.; Kaluza, M.C.; Karsch, S.; Lancaster, K.L.; Mori, W.B.; Najmudin, Z.; et al. Reply to the Comment on "Collimated Multi-MeV Ion Beams from High-Intensity Laser Interactions with Underdense Plasma". *Phys. Rev. Lett.* **2007**, *98*, 049504. [CrossRef]
10. Yogo, A.; Daido, H.; Bulanov, S.V.; Esirkepov, T.Z.; Nemoto, K.; Oishi, Y.; Nayuki, T.; Fujii, T.; Ogura, K.; Orimo, S.; et al. Laser-driven proton acceleration from a near-critical density target. *J. Phy. Conf. Ser.* **2008**, *112*, 42034. [CrossRef]
11. Willingale, L.; Nagel, S.R.; Thomas, A.; Bellei, C.; Clarke, R.J.; Dangor, A.E.; Heathcote, R.; Kaluza, M.C.; Kamperidis, C.; Kneip, S.; et al. Characterization of High-Intensity Laser Propagation in the Relativistic Transparent Regime through Measurements of Energetic Proton Beams. *Phys. Rev. Lett.* **2009**, *102*, 125002. [CrossRef] [PubMed]

12. Fukuda, Y.; Faenov, A.Y.; Tampo, M.; Pikuz, T.A.; Nakamura, T.; Kando, M.; Hayashi, Y.; Yogo, A.; Sakaki, H.; Kameshima, T.; et al. Energy Increase in Multi-MeV Ion Acceleration in the Interaction of a Short Pulse Laser with a Cluster-Gas Target. *Phys. Rev. Lett.* **2009**, *103*, 165002. [CrossRef] [PubMed]
13. Faenov, A.; Magunov, A.; Pikuz, T.; Skobelev, I.; Giulietti, D.; Betti, S.; Galimberti, M.; Gamucci, A.; Giulietti, A.; Gizzi, L.A.; et al. Non-adiabatic cluster expansion after ultrashort laser interaction. *Laser Part Beams* **2008**, *26*, 69–82. [CrossRef]
14. Matsui, R.; Fukuda, Y.; Kishimoto, Y. Quasimonoenergetic Proton Bunch Acceleration Driven by Hemispherically Converging Collisionless Shock in a Hydrogen Cluster Coupled with Relativistically Induced Transparency. *Phys. Rev. Lett.* **2019**, *122*, 014804. [CrossRef] [PubMed]
15. Willingale, L.; Thomas, A.; Nilson, P.M.; Kaluza, M.C.; Bandyopadhyay, S.; Dangor, A.E.; Evans, R.G.; Fernandes, P.; Haines, M.G.; Kamperidis, C.; et al. Fast Advection of Magnetic Fields by Hot Electrons. *Phys. Rev. Lett.* **2010**, *105*, 095001. [CrossRef]
16. Haberberger, D.; Tochitsky, S.; Fiuza, F.; Gong, C.; Fonseca, R.A.; Silva, L.O.; Mori, W.B.; Joshi, C. Collisionless shocks in laser-produced plasma generate mono energetic high-energy proton beams. *Nat. Phys.* **2012**, *8*, 95. [CrossRef]
17. Helle, M.H.; Gordon, D.F.; Kaganovich, D.; Palastro, J.P.; Ting, A.; Chen, Y. Laser-Accelerated Ions from a Shock-Compressed Gas Foil. *Phys. Rev. Lett.* **2016**, *117*, 165001. [CrossRef]
18. Ting, A.; Hafizi, B.; Helle, M.; Chen, Y.H.; Gordon, D.; Kaganovich, D.; Polyanskiy, M.; Pogorelsky, I.; Babzien, M.; Miao, C.; et al. Staging and Laser Acceleration of Ions in Under dense Plasma. In *AIP Conference Proceedings*; AIP Publishing: Melville, NY, USA, 2017; p. 020001.
19. Wan, Y.; Andriyash, I.A.; Hua, J.F.; Pai, C.-H.; Lu, W.; Mori, W.B.; Joshi, C.; Malka, V. Two-stage laser acceleration of high quality protons using a tailored density plasma. *Phys. Rev. Accel. Beams* **2019**, *22*, 021301. [CrossRef]
20. Pak, A.; Kerr, S.; Lemos, N.; Link, A.; Patel, P.; Albert, F.; Divol, L.; Pollock, B.B.; Haberberger, D.; Froula, D.; et al. Collisionless shock acceleration of narrow energy spread ion beams from mixed species plasmas using 1 μm lasers. *Phys. Rev. Accel. Beams* **2018**, *21*, 103401. [CrossRef]
21. Shen, X.F.; Qiao, B.; Zhang, H.; Xie, Y.; Kar, S.; Borghesi, M.; Zepf, M.; Zhou, C.T.; Zhu, S.P.; He, X.T. Electrostatic capacitance-type acceleration of ions with an intense few-cycle laser pulse. *Appl. Phys. Lett.* **2019**, *114*, 144102. [CrossRef]
22. Margarone, D.; Klimo, O.; Kim, I.J.; Prokupek, J.; Limpouch, J.; Jeong, T.M.; Mocek, T.; Psikal, J.; Kim, H.T.; Proska, J.; et al. Laser-Driven Proton Acceleration Enhancement by Nanostructured Foils. *Phys. Rev. Lett.* **2012**, *109*, 234801. [CrossRef] [PubMed]
23. Betti, S.; Cecchetti, C.A.; Förster, E.; Gamucci, A.; Giulietti, A.; Giulietti, D.; Kämpfer, T.; Köster, P.; Labate, L.; Levato, T.; et al. On the effect of rear-surface dielectric coatings on laser-driven proton acceleration. *Phys. Plasmas* **2009**, *16*, 100701. [CrossRef]
24. National Center for Cancer Hadrontherapy (CNAO). Available online: https://fondazionecnao.it/it/ (accessed on 5 August 2019).
25. Cirrone, G.; Cuttone, G.; Lojacono, R.; Nigro, S.L.; Mongelli, V.; Patti, I.V.; Privitera, G.; Raffaele, L.; Rifuggiato, D.; Sabini, M.; et al. A 62 MeV proton beam for the treatment of ocular melanoma at Laboratori Nazionali del Sud-INFN (CATANIA). In *2003 IEEE Nuclear Science Symposium. Conference Record (IEEE Cat. No. 03CH37515)*; IEEE: Piscataway, NJ, USA, 2004; pp. 3658–3662.
26. Barberio, M.; Antici, P. Laser-PIXE using laser-accelerated proton beams. *Sci. Rep.* **2019**, *9*, 6855. [CrossRef] [PubMed]
27. Ryan, C.G. Quantitative trace element imaging using PIXE and the nuclear microprobe. *Int. J. Imaging Syst. Technol.* **2001**, *11*, 219–230. [CrossRef]
28. Labate, L.; Köster, P.; Levato, T.; Gizzi, L.A. A novel technique for single-shot energy-resolved 2D x-ray imaging of plasmas relevant for the inertial confinement fusion. *Rev. Sci. Instrum.* **2012**, *83*, 103504. [CrossRef] [PubMed]
29. Levato, T.; Labate, L.; Pathak, N.; Cecchetti, C.; Koester, P.; Di Fabrizio, E.; Delogu, P.; Giulietti, A.; Giulietti, D.; Gizzi, L.A. Pin-hole array production and detailed data analysis for advanced single-shot X-ray imaging of laboratory plasmas. *Nucl. Instrum. Methods Phys. Res. Sect. A* **2010**, *623*, 842–844. [CrossRef]

30. Romano, F.P.; Caliri, C.; Cosentino, L.; Gammino, S.; Mascali, D.; Pappalardo, L.; Rizzo, F.; Scharf, O.; Santos, H.C. Micro X-ray Fluorescence Imaging in a Tabletop Full Field-X-ray Fluorescence Instrument and in a Full Field-Particle Induced X-ray Emission End Station. *Anal. Chem.* **2016**, *88*, 9873–9880. [CrossRef]
31. Zamponi, F.; Lübcke, A.; Kämpfer, T.; Uschmann, I.; Förster, E.; Robinson, A.P.L.; Giulietti, A.; Köster, P.; Labate, L.; Levato, T.; et al. Directional Bremsstrahlung from a Ti Laser-Produced X-Ray Sourceat Relativistic Intensities in the 3–12 keV Range. *Phys. Rev. Lett.* **2010**, *105*, 085001. [CrossRef]
32. Zamponi, F.; Lübcke, A.; Kämpfer, T.; Uschmann, I.; Förster, E.; Robinson, A.P.L.; Giulietti, A.; Köster, P.; Labate, L.; Levato, T.; et al. Detailed analysis of events from high-energy X-ray photons impinging on a two-phase front-illuminated CCD. *Nucl. Instrum. Methods Phys. Res. A* **2008**, *592*, 346–353.
33. Labate, L.; Levato, T.; Galimberti, M.; Giulietti, A.; Giulietti, D.; Sanna, M.; Traino, C.; Lazzeri, M.; Gizzi, L.A. A single-photon CCD-based setup for in situ measurement of the X-ray spectrum of mammographic units. *Nucl. Instrum. Methods Phys. Res. Sect. A* **2008**, *594*, 278–282. [CrossRef]
34. Gizzi, L.A.; Anania, M.P.; Gatti, G.; Giulietti, D.; Grittani, G.; Kando, M.; Krus, M.; Labate, L.; Levato, T.; Oishi, Y.; et al. Acceleration with self-injection for an all-optical radiation source at LNF. *Nucl. Instrum. Methods Phys. Res. B* **2013**, *309*, 202–209. [CrossRef]
35. Labate, L.; Andreassi, M.G.; Baffigi, F.; Bizzarri, R.; Borghini, A.; Bussolino, G.C.; Fulgentini, L.; Ghetti, F.; Giulietti, A.; Köster, P.; et al. LESM: A laser-driven sub-MeV electron source delivering ultra-high dose rate on thin biological samples. *J. Phys. D Appl. Phys.* **2016**, *49*, 275401. [CrossRef]
36. Koester, P.; Bussolino, G.C.; Cristoforetti, G.; Faenov, A.; Giulietti, A.; Giulietti, D.; Labate, L.; Levato, L.; Pikuz, T.; Gizzi, L.A. High-charge divergent electron beam generation from high-intensity laser interaction with a gas-cluster target. *Laser Part. Beams* **2015**, *33*, 331–338. [CrossRef]
37. Gizzi, L.A.; Cecchetti, C.A.; Giulietti, A.; Giulietti, D.; Koester, P.; Labate, L.; Levato, T.; Pathak, N. Thomson Scattering Imaging from Ultrashort Ultraintense Laser Interaction with Gas. *IEEE Trans. Plasma Sci.* **2011**, *39*, 2954–2955. [CrossRef]
38. Thoss, A.; Richardson, M.; Korn, G.; Faubel, M.; Stiel, H.; Vogt, U.; Elsaesser, T. Kilohertz sources of hard x rays and fast ions with femtosecond laser plasmas. *J. Opt. Soc. Am. B* **2003**, *20*, 224–228. [CrossRef]
39. Morrison, J.T.; Feister, S.; Frische, K.D.; Austin, D.R.; Ngirmang, G.K.; Murphy, N.R.; Orban, C.; A Chowdhury, E.; Roquemore, W.M. MeV proton acceleration at kHz repetition rate from ultra-intense laser liquid interaction. *New J. Phys.* **2018**, *20*, 022001. [CrossRef]
40. Extreme Light Infrastructure. Available online: https://eli-laser.eu/media/1019/eli-whitebook.pdf (accessed on 5 August 2019).
41. Margarone, D.; Cirrone, G.A.P.; Cuttone, G.; Amico, A.; Andò, L.; Borghesi, M.; Bulanov, S.S.; Bulanov, S.V.; Chatain, D.; Fajstavr, A.; et al. ELIMAIA: A Laser-Driven Ion Accelerator for Multidisciplinary Applications. *Quantum Beam Sci.* **2018**, *2*, 8. [CrossRef]
42. Levato, T.; Bonora, S.; Grittani, G.M.; Lazzarini, C.M.; Nawaz, M.F.; Nevrkla, M.; Villanova, L.; Ziano, R.; Bassanese, S.; Bobrova, N.; et al. HELL: High-Energy Electrons by Laser Light, a User-Oriented Experimental Platform at ELI Beamlines. *Appl. Sci.* **2018**, *8*, 1565. [CrossRef]
43. Arber, T.D.; Bennett, K.; Brady, C.S.; Lawrence-Douglas, A.; Ramsay, M.G.; Sircombe, N.J.; Gillies, P.; Evans, R.G.; Schmitz, H.; Bell, A.R.; et al. Contemporary particle-in-cell approach to laser-plasma modelling. *Plasma Phys. Control. Fusion* **2015**, *57*, 113001. [CrossRef]
44. Park, J.; Bulanov, S.S.; Bin, J.; Ji, Q.; Steinke, S.; Vay, J.L.; Geddes, C.G.R.; Schoreder, C.B.; Leemans, W.P.; Schenkel, T.; et al. Ion Acceleration in Laser Generated Mega Tesla Magnetic Vortex. *arXiv* **2019**, arXiv:1904.03281.